International Journal of Power and Energy Systems, Vol. 46, No. 10, 2026
An Open Access Paper

HIGH PRECISION STATE OF CHARGE ESTIMATION FOR LITHIUM-ION BATTERIES USING AN INTERMEDIATE OBSERVER

Dan Wang,* Sicheng Zhou,* Zhibo Feng,* Jun Wu,* and Guanjie Wang**

Abstract

An intermediate observer that no longer requires the observer-matching condition is proposed for real-time state-of-charge (SoC) estimation of lithium-ion batteries under dynamic operation. Built upon a dual-polarization RC equivalent-circuit model, the algorithm introduces an intermediate variable to generate a residual that compensates for model errors, measurement noise and ageing disturbances online. Lyapunov analysis proves that the estimation error is uniformly ultimately bounded, while the computational burden is noticeably lower than that of conventional sliding-mode or high-gain observers. Neware bench tests show a maximum error of 1.5 % under noise-free conditions, 53 % lower than the H_∞ method, and only 2.8 % when 0.1 A sensor noise is injected, still outperforming the comparison methods. Without offline training, large datasets, or observer-matching conditions, the scheme is readily deployed in embedded battery management systems and offers a robust, lightweight SoC solution for diverse lithium-ion chemistries.

Key Words

Lithium-ion battery, state of charge (SoC), intermediate observer, H_∞ technology, SoC estimation

1. Introduction

As the global energy transition and sustainable development accelerate, lithium-ion batteries have emerged as a preferred choice in the fields of new energy and energy storage due to their exceptional performance [1], [2]. With advantages such as high energy density, light weight, minimal memory effect, low self-discharge and a cycle life that can exceed thousands of cycles under proper conditions, lithium-ion batteries stand out among various energy storage technologies [3], [5]. Additionally, their fast-charging capability significantly enhances system efficiency and aligns with the principles of environmental protection and sustainable development [6]. In recent years, lithium-ion batteries have been widely applied in critical sectors such as electric vehicles, smart grids, and the aerospace industry, becoming a key driving force for the development of related industries [7], [10].

In the application of lithium-ion batteries, precise estimation of the state of charge (SoC) is critical [11], [12]. As a core function of the battery management system (BMS), the accuracy of SoC estimation directly determines the efficiency of energy distribution and the safety boundaries of the battery system [13]. However, SoC is an indicator of the remaining usable charge relative to the nominal capacity, and its accurate estimation is complicated by coupled electrochemical processes of the battery and cannot be directly measured using traditional sensors [14]. The accuracy of SoC estimation is influenced by a combination of factors, including model errors, noise interference, and battery- ageing effects [15], [16]. Therefore, achieving high-precision and robust SoC estimation under dynamic operating conditions and complex interference environments has become a common challenge that urgently needs to be addressed in both academia and industry [17], [18].

Currently, SoC-estimation methods are mainly divided into two categories. The simpler estimation methods include the ampere-hour integration method and the open-circuit-voltage method. The ampere-hour integration method relies on the selection of an initial value and is prone to cumulative errors caused by initial inaccuracies and measurement errors, making it difficult to achieve accurate online estimation [19]. The open-circuit-voltage method, while capable of accurately estimating the SoC value under non-operating conditions, requires the battery to be left idle for a long time to obtain the open-circuit voltage. It cannot meet real-time requirements and is therefore

* Marketing Service Center, State Grid Liaoning Electric Power Co. Ltd., Shenyang Liaoning, P.R. China; e-mail: wangd2012@163.com, 76939965@qq.com, fzb1995@foxmail.com, 527610050@qq.com
** Zhejiang Key Laboratory of Advanced Solid State Energy Storage Technology and Applications, Taizhou Institute of Zhejiang University, Taizhou, Zhejiang, P.R. China; e-mail: gjwang@zju.edu.cn
Corresponding author: Dan Wang

Recommended by: Ahmed Abdelrahman
(DOI: 10.2316/J.2026.203-0655)

not suitable for online real-time estimation in dynamic environments [20]. To overcome these shortcomings, methods based on equivalent-circuit models and data-driven approaches have emerged [1], [21], [22].

Building on this, an improved composite-kernel Gaussian process regression (GPR) that incorporates ageing data was developed, eliminating the shortcomings of the traditional single-kernel GPR model and offering greater versatility [23]. Another approach enriched the input-feature set by adding average power and average resistance, yielding more accurate and robust SoC characterisation [24]. Although such data-driven techniques can deliver high accuracy, they require large offline data sets, involve lengthy training, and are strongly dependent on the chosen training strategy, making adaptation to battery ageing difficult [14], [25]. Consequently, attention has returned to model-based techniques [26], [28].

For rechargeable-battery health monitoring, an extended Kalman filter (EKF) that fuses ultrasonic signals decomposed by empirical-mode decomposition, grounded in Biot theory, attains high-precision real-time SoC estimates with lower error than the conventional EKF [29]. Sliding-mode observers, implemented as three-terminal observers, lower computational load yet introduce chattering that degrades accuracy [30]. Moreover, to address potential external disturbances in the system, the robustness of the method is critical [6]. H_∞ technology and high-gain robust observers have played important roles in enhancing robustness [6], [31], but these methods still exhibit some conservatism, leaving room for further performance improvement.

To address these unresolved issues, this paper proposes a novel intermediate-observer-based SoC estimation method with three distinct innovations that distinguish it from existing work:

(1) Breaking the observer-matching condition constraint: Unlike conventional observer-based methods [18], [30], the proposed intermediate observer only requires bounded lumped disturbances, a mild assumption that is easily satisfied in practice for all lithium-ion batteries. This eliminates the dependency on strict matching conditions, enabling direct application to diverse battery chemistries without modifying the observer structure.

(2) Online residual compensation via intermediate variables: A unique intermediate variable is introduced to generate real-time residuals, which synchronously offset model nonlinearities, measurement noise, and ageing-induced performance degradation. This avoids the conservatism of traditional H_∞ observers and the chattering of sliding-mode observers, achieving a balanced improvement in accuracy and robustness.

(3) Lightweight design for embedded deployment: By integrating a dual-polarization RC model with the simplified intermediate observer structure, the method avoids large offline datasets and complex computations. It thus addresses the high computational burden of EKF [29] and data-driven methods, making it readily deployable in embedded BMS.

Simulation and experimental results confirm that the proposed method not only achieves high-precision and robust SoC estimation but also offers broader applicability and practical value, providing a new solution for SoC estimation in lithium-ion batteries under dynamic and complex operating conditions.

2. Battery Equivalent Circuit Model

To achieve higher SoC estimation accuracy, this work considers an equivalent circuit model with a dual-polarization RC circuit, which balances the complexity and precision of the electrochemical behaviour of lithium-ion batteries, as shown in Fig. 1. In the figure, R_0 is the internal resistance of the lithium-ion battery. The two RC networks (R_p, C_p) and (R_e, C_e) respectively describe the fast electrochemical and slow concentration polarization reactions of the lithium-ion battery. R_p and C_p represent the concentration polarization resistance and capacitance, while R_e and C_e represent the electrochemical polarization resistance and capacitance. The voltages across R_0, R_p, and R_e are U_0, U_p, and U_e, respectively, and I is the current. U_{OC} is the open-circuit voltage, and U is the terminal voltage of the battery.

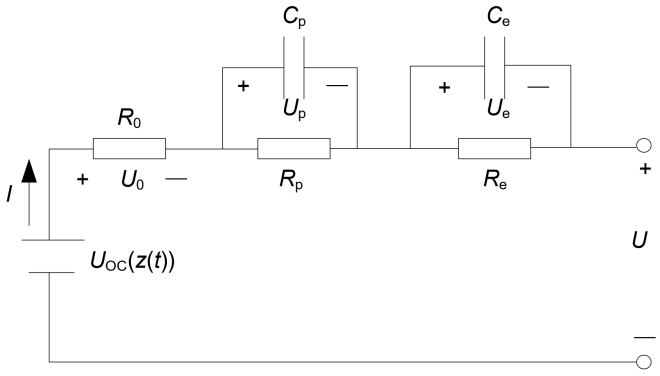

Figure 1. Battery Equivalent Circuit Model.

The SoC of a lithium-ion battery at time t is defined as:

$$SoC\,(t) = SoC\,(0) - \frac{\eta}{Q_n}\int_0^t I\,(\tau)\,d\tau \tag{1}$$

where $SoC\,(0)$ is the initial SoC, $0 < \eta \leq 1$ is the coulombic efficiency, and Q_n is the nominal capacity of the battery.

According to Kirchhoff's law, the voltage across a lithium-ion battery is:

$$U\,(t) = U_{\mathrm{OC}}\,(z\,(t)) - R_0 I\,(t) - U_p\,(t) - U_e\,(t) \tag{2}$$

where $U_{\mathrm{OC}}\,(z\,(t)) = \sum_{i=0}^{N} \ell_i z^i\,(t)$ is the open-circuit voltage, and ℓ_i is the i-th polynomial fitting coefficient. When $N \geq 12$, the model's precision improvement potential drops sharply, to reduce unnecessary computational complexity, a value of $N = 12$ is chosen [3].

The two polarization reactions can be respectively described as:

$$\frac{dU_p\,(t)}{dt} = -\frac{1}{R_p C_p} U_p\,(t) + \frac{1}{C_p} I\,(t) \tag{3}$$

$$\frac{dU_e(t)}{dt} = -\frac{1}{R_e C_e} U_e(t) + \frac{1}{C_e} I(t) \tag{4}$$

The relationship between the SoC of a lithium-ion battery, $z(t)$, the current, and the nominal capacity is:

$$\frac{dz(t)}{dt} = -\frac{\eta}{Q_n} I(t) \tag{5}$$

From (2), we can derive:

$$I(t) = \frac{U_{\mathrm{OC}}(z(t)) - U_p(t) - U_e(t) - U(t)}{R_0} \tag{6}$$

Substituting into (5) gives:

$$\begin{aligned}\frac{dz(t)}{dt} = -\frac{\eta}{Q_n} I(t) = &-\frac{\eta}{Q_n R_0} U_{\mathrm{OC}}(z(t)) + \frac{\eta}{Q_n R_0} U_p(t) \\ &+ \frac{\eta}{Q_n R_0} U_e(t) + \frac{\eta}{Q_n R_0} U(t)\end{aligned} \tag{7}$$

Given that the current variation between samples is minimal, we can assume $\frac{dI(t)}{dt} \approx 0$. Then, from (2), we also obtain:

$$\begin{aligned}\frac{\mathrm{d}U(t)}{\mathrm{d}t} &= \frac{\partial U_{\mathrm{oc}}(z(t))}{\partial z(t)} \frac{\mathrm{d}z(t)}{\mathrm{d}t} - R_0 \frac{\mathrm{d}I(t)}{\mathrm{d}t} \\ &\quad - \frac{\mathrm{d}U_{\mathrm{p}}(t)}{\mathrm{d}t} - \frac{\mathrm{d}U_{\mathrm{e}}(t)}{\mathrm{d}t} \\ &= -\frac{\eta I(t)}{Q_{\mathrm{p}}} \frac{\partial U_{\mathrm{oc}}(z(t))}{\partial z(t)} + \frac{1}{R_{\mathrm{p}} C_{\mathrm{p}}} U_{\mathrm{p}}(t) - \frac{1}{C_{\mathrm{p}}} I(t) \\ &\quad + \frac{1}{R_{\mathrm{e}} C_{\mathrm{e}}} U_{\mathrm{e}}(t) - \frac{1}{C_{\mathrm{e}}} I(t)\end{aligned} \tag{8}$$

Using (2) again, we get:

$$U_e(t) = U_{\mathrm{OC}}(z(t)) - R_0 I(t) - U_p(t) - U(t) \tag{9}$$

Thus, it follows that:

$$\begin{aligned}\frac{\mathrm{d}U(t)}{\mathrm{d}t} &= \frac{\partial U_{\mathrm{oc}}(z(t))}{\partial z(t)} \frac{\mathrm{d}z(t)}{\mathrm{d}t} - \frac{\mathrm{d}U_{\mathrm{p}}(t)}{\mathrm{d}t} - \frac{\mathrm{d}U_{\mathrm{e}}(t)}{\mathrm{d}t} - R_{\mathrm{e}} \frac{\mathrm{d}(t)}{\mathrm{d}t} \\ &= -\frac{\eta I(t)}{Q_{\mathrm{n}}} \frac{\partial U_{\mathrm{oc}}(z(t))}{\partial z(t)} + \frac{U_{\mathrm{p}}(t)}{R_{\mathrm{p}} C_{\mathrm{p}}} - \frac{I(t)}{C_{\mathrm{p}}} + \frac{1}{R_{\mathrm{e}} C_{\mathrm{e}}} \\ &\quad (U_{\mathrm{OC}}(z(t)) - R_{\mathrm{e}} I(t) - U_{\mathrm{p}}(t) - U(t)) - \frac{I(t)}{C_{\mathrm{e}}} \\ &= -\frac{\eta I(t)}{Q_{\mathrm{n}}} \frac{\partial U_{\mathrm{oc}}(z(t))}{\partial z(t)} + \frac{U_{\mathrm{p}}(t)}{R_{\mathrm{p}} C_{\mathrm{p}}} - \frac{I(t)}{C_{\mathrm{p}}} + \frac{1}{R_{\mathrm{e}} C_{\mathrm{e}}} U_{\mathrm{oc}}(z(t)) \\ &\quad - \frac{1}{R_{\mathrm{e}} C_{\mathrm{e}}} R_{\mathrm{e}} I(t) - \frac{1}{R_{\mathrm{e}} C_{\mathrm{e}}} U_{\mathrm{p}}(t) - \frac{1}{R_{\mathrm{e}} C_{\mathrm{e}}} U(t) - \frac{I(t)}{C_{\mathrm{e}}} \\ &= \frac{1}{R_{\mathrm{e}} C_{\mathrm{e}}} U_{\mathrm{oc}}(z(t)) - \frac{1}{R_{\mathrm{e}} C_{\mathrm{e}}} U(t) + \left(\frac{1}{R_{\mathrm{p}} C_{\mathrm{p}}} - \frac{1}{R_{\mathrm{e}} C_{\mathrm{e}}} \right) \\ &\quad U_{\mathrm{p}}(t) - \left(\frac{\eta}{Q_{\mathrm{n}}} \frac{\partial U_{\mathrm{oc}}(z(t))}{\partial z(t)} + \frac{1}{C_{\mathrm{p}}} + \frac{1}{R_{\mathrm{e}} C_{\mathrm{e}}} R_0 + \frac{1}{C_{\mathrm{e}}} \right) I(t)\end{aligned} \tag{10}$$

From this, the system's state-space representation can be established as:

$$\begin{aligned}\begin{bmatrix} \dot{U}(t) \\ \dot{z}(t) \\ \dot{U}_{\mathrm{p}}(t) \\ \dot{U}_{\mathrm{e}}(t) \end{bmatrix} &= \begin{bmatrix} -\frac{1}{R_{\mathrm{e}} C_{\mathrm{e}}} & \frac{1}{R_{\mathrm{e}} C_{\mathrm{e}}} \ell & \frac{1}{R_{\mathrm{p}} C_{\mathrm{p}}} - \frac{1}{R_{\mathrm{e}} C_{\mathrm{e}}} & 0 \\ \frac{\eta}{R_0 Q_{\mathrm{n}}} & \frac{1}{R_0 Q_{\mathrm{n}}} \ell & \frac{\eta}{R_0 Q_{\mathrm{n}}} & \frac{\eta}{R_{\mathrm{a}} Q_{\mathrm{n}}} \\ 0 & 0 & -\frac{1}{R_{\mathrm{p}} C_{\mathrm{p}}} & 0 \\ 0 & 0 & 0 & -\frac{1}{R_{\mathrm{e}} C_{\mathrm{e}}} \end{bmatrix} \\ &\quad \begin{bmatrix} U(t) \\ z(t) \\ U_{\mathrm{p}}(t) \\ U_{\mathrm{e}}(t) \end{bmatrix} + \begin{bmatrix} -\frac{1}{C_{\mathrm{p}}} - \frac{1}{C_{\mathrm{e}}} - \frac{1}{R_{\mathrm{e}} C_{\mathrm{e}}} R_{\mathrm{e}} \\ 0 \\ \frac{1}{C_{\mathrm{p}}} \\ \frac{1}{C_{\mathrm{e}}} \end{bmatrix} I(t) \\ &\quad + \begin{bmatrix} \frac{1}{R_{\mathrm{e}} C_{\mathrm{e}}} U_{\mathrm{oc}}(z(t)) - \frac{1}{R_{\mathrm{e}} C_{\mathrm{e}}} \ell(t) - \frac{\eta I(t)}{Q_{\mathrm{n}}} \frac{\partial U_{\mathrm{oc}}(z(t))}{\partial z(t)} \\ -\frac{\eta}{R_0 Q_{\mathrm{n}}} U_{\mathrm{oc}}(z(t)) - \frac{1}{R_0 Q_{\mathrm{n}}} \ell z(t) \\ 0 \\ 0 \end{bmatrix}\end{aligned} \tag{11}$$

Select the system state as $x(t) = \begin{bmatrix} U(t) & z(t) & U_p(t) & U_e(t) \end{bmatrix}^T$, the control input as $u(t) = I(t)$, and the output as the terminal voltage $U(t) = \begin{bmatrix} 1 & 0 & 0 & 0 \end{bmatrix} \begin{bmatrix} U(t) & z(t) & U_p(t) & U_e(t) \end{bmatrix}^T$.

The output equation can be established as:

$$y(t) = Cx(t) \tag{12}$$

where $C = \begin{bmatrix} 1 & 0 & 0 & 0 \end{bmatrix}$.

Considering external unknown disturbances $d_1(t)$ and measurement noise $d_2(t)$ that may occur in the system, system (10) can be rewritten as:

$$\begin{cases} \dot{x}(t) = Ax(t) + Bu(t) + \phi(x(t), u(t)) + Dd_1(t) \\ y(t) = Cx(t) + Fd_2(t) \end{cases} \tag{13}$$

where, $A = \begin{bmatrix} -\frac{1}{R_e C_e} & \frac{1}{R_e C_e} \ell & \frac{1}{R_p C_p} - \frac{1}{R_e C_e} & 0 \\ \frac{\eta}{R_0 Q_n} & \frac{1}{R_0 Q_n} \ell & \frac{\eta}{R_0 Q_n} & \frac{\eta}{R_0 Q_n} \\ 0 & 0 & -\frac{1}{R_p C_p} & 0 \\ 0 & 0 & 0 & -\frac{1}{R_e C_e} \end{bmatrix}$, $B = \begin{bmatrix} -\frac{1}{C_p} - \frac{1}{C_e} - \frac{1}{R_e C_e} R_0 \\ 0 \\ \frac{1}{C_p} \\ \frac{1}{C_e} \end{bmatrix}$, $\phi(x(t), u(t)) = \begin{bmatrix} \frac{1}{R_e C_e} U_{\mathrm{OC}}(z(t)) - \frac{1}{R_e C_e} \ell z(t) - \frac{\eta I(t)}{Q_n} \frac{\partial U_{\mathrm{OC}}(z(t))}{\partial z(t)} \\ -\frac{\eta}{R_0 Q_n} U_{\mathrm{OC}}(z(t)) - \frac{1}{R_0 Q_n} \ell z(t) \\ 0 \\ 0 \end{bmatrix}$, and D and F are known coefficient matrices with appropriate dimensions.

Remark 1. $\phi(x(t), u(t))$ is derived from the dual-polarization RC equivalent-circuit model and is designed to capture the nonlinear dynamics and coupled electrochemical behaviours of lithium-ion batteries that are not fully described by the linear state-space framework Eq. (11). Its core physical implications include: The nonlinear dependence of the open-circuit voltage U_{OC} on SoC; The temperature-dependent variations of polarization resistances and capacitances; The weak electrochemical coupling effect between fast and slow polarization reactions; Ageing-related nonlinearities, etc. Thus, an appropriate $\phi(x(t), u(t))$ is indispensable for improving estimation accuracy, as it bridges the gap between the simplified linear model and the real complex battery dynamics.

Let $X(t) = \begin{bmatrix} x(t) & d_2(t) \end{bmatrix}^T$, $\Gamma = \begin{bmatrix} A & 0 \\ 0 & 0 \end{bmatrix}, \gamma = \begin{bmatrix} B \\ 0 \end{bmatrix}$, $\Xi = \begin{bmatrix} I \\ 0 \end{bmatrix}$, $\Theta = \begin{bmatrix} D \\ 0 \end{bmatrix}$, $\Psi = \begin{bmatrix} 0 \\ I \end{bmatrix}$, $\Phi = [C \quad F]$ then system (13) can be rewritten as:

$$\begin{cases} \dot{X}(t) &= \Gamma X(t) + \Upsilon u(t) \quad +\Xi\phi\left(\Xi^T X(t), u(t)\right) \\ & \qquad\qquad\quad +\Theta d_1(t) + \Psi \dot{d}_2(t) \\ y(t) &= \Phi X(t) \end{cases} \tag{14}$$

It is evident that due to the presence of the unknown terms $d_1(t)$ and $d_2(t)$, conventional methods often require assumptions that all these terms are bounded. Some methods even require knowledge of their specific bounds. In contrast, the approach proposed in this paper only assumes that $\dot{d}_2(t)$ is bounded, which is an assumption that is objectively acceptable.

Remark 2. Current sensors (e.g., shunts, Hall effect sensors) employed for SoC estimation in practical BMS are inherently limited by bandwidth and slew rate. Taking the built-in sensor of the Neware CT4991-60V-30A tester used in this experiment as an example, its noise amplitude typically ranges from ±0.1 A to ±0.5 A (consistent with the injected 0.1 A noise). The noise slew rate is constrained by the sensor bandwidth (1–10 kHz), leading to the derivation that $\left|\dot{d}_2(t)\right| \leq 10$ A/s, thus ensuring inherent boundedness. During the dynamic operation of electric vehicles or energy storage systems, the battery current is restricted by physical limits (the Samsung INR18650-29E battery has a maximum charge/discharge rate $\leq$ 1C), resulting in smooth variations. Even after superimposing sensor noise, the current slew rate cannot exceed the sensor's dynamic response capability, further confirming the boundedness of $\dot{d}_2(t)$.

Remark 3. A dual-polarization RC equivalent-circuit model is adopted, which only characterizes the common electrochemical behaviours of lithium-ion batteries (internal resistance, electrochemical polarization, concentration polarization) and is independent of specific chemical systems. For lithium cobalt oxide (LCO), lithium iron phosphate (LFP), nickel-cobalt-manganese ternary (NCM), or nickel-cobalt-aluminum (NCA) batteries, accurate modeling can be achieved by adjusting model parameters $R_\mathrm{p}, C_\mathrm{p}, R_\mathrm{e}, C_\mathrm{e}$ without modifying the model structure.

3. Intermediate Observer Design

Define an intermediate variable $\varphi(t) = d_1(t) - s\theta^\mathrm{T} X(t)$, and assume that the Lipschitz constant of the nonlinear part $\phi(x(t), u(t))$ is γ. The following intermediate observer is proposed:

$$\begin{cases} \dot{\hat{X}}(t) = \Gamma\hat{X}(t) + \Upsilon u(t) + \Xi\phi\left(\Xi^\mathrm{T}\hat{X}(t), u(t)\right) \\ \qquad\qquad\qquad +\Theta\tilde{d}_1(t) + L(y(t) - \Phi\tilde{X}(t)) \\ \dot{\hat{\varphi}}(t) = -\xi\Theta^\mathrm{T}\left(\Gamma\hat{X}(t) + \Upsilon u(t) + \Xi\phi\left(\Xi^\mathrm{T}\hat{X}(t), u(t)\right)\right. \\ \qquad\qquad\qquad \left. +\xi\Theta^\mathrm{T}\hat{X}(t)\right) - \xi\Theta^\mathrm{T}\Theta\tilde{\varphi}(t) \\ \hat{\dot{d}}_1(t) = \hat{\varphi}(t) + \xi\Theta^\mathrm{T}\hat{X}(t) \end{cases} \tag{15}$$

where, $\square(t)$ is the estimate of $\square(t)$, $\tilde{\square}(t)$ are $X(t), d_1(t), \varphi(t), d_2(t)$ respectively, and we have $\hat{d}_2(t) = \Psi^\mathrm{T} X(t)$. Define the observer residual as:

$$\varepsilon_X(t) = X(t) - \hat{X}(t) \tag{16}$$

$$\varepsilon_\varphi(t) = \varphi(t) - \hat{\varphi}(t) \tag{17}$$

$$\begin{aligned} \varepsilon_{d_1}(t) &= d_1(t) - \hat{d}_1(t) \\ &= \varphi(t) + \xi\Theta^\mathrm{T} X(t) - \hat{\varphi}(t) - \xi\Theta^\mathrm{T}\hat{X}(t) \\ &= \varepsilon_\varphi(t) + \xi\Theta^\mathrm{T}\varepsilon_X(t) \end{aligned} \tag{18}$$

It can be easily shown that:

$$\begin{aligned} \dot{\varepsilon}_X(t) &= \dot{X}(t) - \dot{\hat{X}}(t) \\ &= \Gamma X(t) + \Upsilon u(t) + \Xi\phi\left(\Xi^\mathrm{T} X(t), u(t)\right) \\ &+\Theta d_1(t) + \Psi\dot{d}_2(t) - \Gamma\hat{X}(t) - \Upsilon u(t) \\ &-\Xi\phi\left(\Xi^\mathrm{T}\hat{X}(t), u(t)\right) - \Theta\hat{d}_1(t) - L(y(t) - \Phi\hat{X}(t)) \\ &= (\Gamma - L\Phi)\varepsilon_X(t) + \Xi\varepsilon_\phi + \Theta\varepsilon_{d_1}(t) + \Psi\dot{d}_2(t) \\ &= (\Gamma - L\Phi)\varepsilon_X(t) + \Xi\varepsilon_\phi + \Theta\left(\varepsilon_\phi(t) + \xi\Theta^\mathrm{T}\varepsilon_X(t)\right) \\ &+\Psi\dot{d}_2(t) \\ &= \left(\Gamma - L\Phi + \xi\Theta\Theta^\mathrm{T}\right)\varepsilon_X(t) + \Xi\varepsilon_\phi \\ &+\Theta\varepsilon_\phi(t) + \Psi\dot{d}_2(t) \end{aligned} \tag{19}$$

where $\varepsilon_\phi = \phi\left(\Xi^\mathrm{T} X(t), u(t)\right) - \phi\left(\Xi^\mathrm{T}\hat{X}(t), u(t)\right), \|\varepsilon_\phi\| \leq \gamma\|\varepsilon_X(t)\|$.
While:

$$\begin{aligned} \dot{\varepsilon}_\varphi(t) &= \dot{\varphi}(t) - \dot{\hat{\varphi}}(t) \\ &= \dot{d}_1(t) - \xi\Theta^\mathrm{T}\dot{X}(t) + \xi\Theta^\mathrm{T}\left(\Gamma\hat{X}(t) + \Upsilon u(t)\right. \\ &\left.+\Xi\phi\left(\Xi^\mathrm{T}\hat{X}(t), u(t)\right) + \xi\Theta^\mathrm{T}\hat{X}(t)\right) + \xi\Theta^\mathrm{T}\Theta\hat{\varphi}(t) \\ &= \dot{d}_1(t) - \xi\Theta^\mathrm{T}\left(\Gamma X(t) + \Upsilon u(t) + \Xi\phi\left(\Xi^\mathrm{T} X(t), u(t)\right)\right. \\ &\left.+\Theta d_1(t) + \Psi\dot{d}_2(t)\right) + \xi\Theta^\mathrm{T}\left(\Gamma\hat{X}(t) + \Upsilon u(t)\right. \\ &\left.+\Xi\phi\left(\Xi^\mathrm{T}\hat{X}(t), u(t)\right) + \xi\Theta^\mathrm{T}\hat{X}(t)\right) + \xi\Theta^\mathrm{T}\Theta\hat{\varphi}(t) \\ &= \dot{d}_1(t) - \xi\Theta^\mathrm{T}\Gamma\varepsilon_X(t) - \xi\Theta^\mathrm{T}\Xi\varepsilon_\phi - \xi\Theta^\mathrm{T}\Theta d_1(t) \\ &-\xi\Theta^\mathrm{T}\Psi\dot{d}_2(t) + \xi\Theta^\mathrm{T}\xi\Theta^\mathrm{T}\hat{X}(t) + \xi\Theta^\mathrm{T}\Theta\hat{\varphi}(t) \\ &= \dot{d}_1(t) - \xi\Theta^\mathrm{T}\Gamma\varepsilon_X(t) - \xi\Theta^\mathrm{T}\Xi\varepsilon_\phi - \xi\Theta^\mathrm{T}\Theta d_1(t) \\ &-\xi\Theta^\mathrm{T}\Psi\dot{d}_2(t) - \xi\Theta^\mathrm{T}\xi\Theta^\mathrm{T} X(t) + \xi\Theta^\mathrm{T}\ell\Theta\Theta^\mathrm{T} X(t) \\ &+\xi\Theta^\mathrm{T}\xi\Theta^\mathrm{T}\hat{X}(t) + \xi\Theta^\mathrm{T}\Theta\hat{\varphi}(t) \\ &= \dot{d}_1(t) - \xi\Theta^\mathrm{T}\Gamma\varepsilon_X(t) - \xi\Theta^\mathrm{T}\Xi\varepsilon_\phi - \xi\Theta^\mathrm{T}\Theta\left(d_1(t)\right. \\ &\left.-\xi\Theta^\mathrm{T} X(t)\right) - \xi\Theta^\mathrm{T}\xi\Theta^\mathrm{T}(X(t) - \hat{X}(t)) + \xi\Theta^\mathrm{T}\Theta\hat{\varphi}(t) \\ &-\xi\Theta^\mathrm{T}\Psi\dot{d}_2(t) \\ &= \dot{d}_1(t) - \xi\Theta^\mathrm{T}\left(\Gamma + \xi\Theta\Theta^\mathrm{T}\right)\varepsilon_X(t) - \xi\Theta^\mathrm{T}\Xi\varepsilon_\phi \\ &-\xi\Theta^\mathrm{T}\Theta\varepsilon_\phi(t) - \xi\Theta^\mathrm{T}\Psi\dot{d}_2(t) \end{aligned} \tag{20}$$

To demonstrate the effectiveness of the observer, it is necessary to analyze the stability of the error system. A Lyapunov function is selected as follows:

$$V(t) = \varepsilon_X^\mathrm{T}(t)P\varepsilon_X(t) + \varepsilon_\varphi^\mathrm{T}(t)\lambda I\varepsilon_\varphi(t) \tag{21}$$

where, $\lambda > 0$ is an arbitrary positive constant to be selected, and it follows that:

$$
\begin{aligned}
\dot{V}(t) &= \dot{\varepsilon}_X^{\mathrm{T}}(t)P\varepsilon_X(t) + \varepsilon_X^{\mathrm{T}}(t)P\dot{\varepsilon}_X(t) + \dot{\varepsilon}_\varphi^{\mathrm{T}}(t)\lambda I\varepsilon_\varphi(t) + \varepsilon_\varphi^{\mathrm{T}}(t)\lambda I\dot{\varepsilon}_\varphi(t) \\
&= \left(\left(\Gamma - L\Phi + \xi\Theta\Theta^{\mathrm{T}}\right)\varepsilon_X(t) + \Xi\varepsilon_\phi + \Theta\varepsilon_\varphi(t) + \Psi\dot{d}_2(t)\right)^{\mathrm{T}} P\varepsilon_X(t) \\
&\quad + \varepsilon_X^{\mathrm{T}}(t)P\left(\left(\Gamma - L\Phi + \xi\Theta\Theta^{\mathrm{T}}\right)\varepsilon_X(t) + \Xi\varepsilon_\phi + \Theta\varepsilon_\varphi(t) + \Psi\dot{d}_2(t)\right) \\
&\quad + \left(\dot{d}_1(t) - \xi\Theta^{\mathrm{T}}\left(\Gamma + \xi\Theta\Theta^{\mathrm{T}}\right)\varepsilon_X(t) - \xi\Theta^{\mathrm{T}}\Xi\varepsilon_\phi - \xi\Theta^{\mathrm{T}}\Theta\varepsilon_\varphi(t) - \xi\Theta^{\mathrm{T}}\Psi\dot{d}_2(t)\right)^{\mathrm{T}}\lambda I\varepsilon_\varphi(t) \\
&\quad + \varepsilon_\varphi^{\mathrm{T}}(t)\lambda I\left(\dot{d}_1(t) - \xi\Theta^{\mathrm{T}}\left(\Gamma + \xi\Theta\Theta^{\mathrm{T}}\right)\varepsilon_X(t) - \xi\Theta^{\mathrm{T}}\Xi\varepsilon_\phi - \xi\Theta^{\mathrm{T}}\Theta\varepsilon_\varphi(t) - \xi\Theta^{\mathrm{T}}\Psi\dot{d}_2(t)\right) \\
&= \varepsilon_X^{\mathrm{T}}(t)\left(\Gamma - L\Phi + \xi\Theta\Theta^{\mathrm{T}}\right)^{\mathrm{T}} P\varepsilon_X(t) + \varepsilon_\phi^{\mathrm{T}}(t)\Xi^{\mathrm{T}}P\varepsilon_X(t) + \varepsilon_\varphi^{\mathrm{T}}(t)\Theta^{\mathrm{T}}P\varepsilon_X(t) + \dot{d}_2^{\mathrm{T}}(t)\Psi^{\mathrm{T}}P\varepsilon_X(t) \\
&\quad + \varepsilon_X^{\mathrm{T}}(t)P\left(\Gamma - L\Phi + \xi\Theta\Theta^{\mathrm{T}}\right)\varepsilon_X(t) + \varepsilon_X^{\mathrm{T}}(t)P\Xi\varepsilon_\phi + \varepsilon_X^{\mathrm{T}}(t)P\Theta\varepsilon_\varphi(t) + \varepsilon_X^{\mathrm{T}}(t)P\Psi\dot{d}_2(t) \\
&\quad + \dot{d}_1^{\mathrm{T}}(t)\lambda I\varepsilon_\varphi(t) - \varepsilon_X^{\mathrm{T}}(t)\left(\Gamma + \xi\Theta\Theta^{\mathrm{T}}\right)^{\mathrm{T}}\xi\Theta\lambda I\varepsilon_\varphi(t) - \varepsilon_\phi^{\mathrm{T}}(t)\Xi^{\mathrm{T}}\Theta\xi\lambda I\varepsilon_\varphi(t) \\
&\quad - \varepsilon_\varphi^{\mathrm{T}}(t)\xi\Theta^{\mathrm{T}}\Theta\lambda I\varepsilon_\varphi(t) - \dot{d}_2^{\mathrm{T}}(t)\Psi^{\mathrm{T}}\xi\Theta\lambda I\varepsilon_\varphi(t) \\
&\quad + \varepsilon_\varphi^{\mathrm{T}}(t)\lambda I\dot{d}_1(t) - \varepsilon_\varphi^{\mathrm{T}}(t)\lambda I\xi\Theta^{\mathrm{T}}\left(\Gamma + \xi\Theta\Theta^{\mathrm{T}}\right)\varepsilon_X(t) - \varepsilon_\varphi^{\mathrm{T}}(t)\lambda I\xi\Theta^{\mathrm{T}}\Xi\varepsilon_\phi(t) \\
&\quad - \varepsilon_\varphi^{\mathrm{T}}(t)\lambda I\xi\Theta^{\mathrm{T}}\Theta\varepsilon_\varphi(t) - \varepsilon_\varphi^{\mathrm{T}}(t)\lambda I\xi\Theta^{\mathrm{T}}\Psi\dot{d}_2(t)
\end{aligned}
$$

A

$$
\Omega = \begin{bmatrix}
\left(\Gamma - L\Phi + \xi\Theta\Theta^{\mathrm{T}}\right)^{\mathrm{T}}P + P\left(\Gamma - L\Phi + \xi\Theta\Theta^{\mathrm{T}}\right) + \left(1+\rho\gamma^2\right)I & * & * & * & * \\
\Xi^{\mathrm{T}}P & -\rho I & * & * & * \\
\Theta^{\mathrm{T}}P - \lambda\xi\Theta^{\mathrm{T}}\left(\Gamma + \xi\Theta\Theta^{\mathrm{T}}\right) & -\lambda I\xi\Theta^{\mathrm{T}}\Xi & -2\xi\lambda\Theta^{\mathrm{T}}\Theta + I & * & * \\
0 & 0 & \lambda I & -\delta^2 I & * \\
\Psi^{\mathrm{T}}P & 0 & -\xi\lambda\Psi^{\mathrm{T}}\Theta & 0 & -\delta^2 I
\end{bmatrix}
$$

,* denote the symmetric entries along the main diagonal. Setting $W = PL$ yields:

$$
\Omega = \begin{bmatrix}
\Gamma^{\mathrm{T}}P - \Phi^{\mathrm{T}}W^{\mathrm{T}} + \xi\Theta\Theta^{\mathrm{T}}P + \left(P\Gamma - W\Phi + P\xi\Theta\Theta^{\mathrm{T}}\right) + \left(1+\rho\gamma^2\right)I & & & & \\
\Xi^{\mathrm{T}}P & -\rho I & & & \\
\Theta^{\mathrm{T}}P - \lambda\xi\Theta^{\mathrm{T}}\Gamma - \lambda\xi\xi\Theta^{\mathrm{T}}\Theta\Theta^{\mathrm{T}} & -\lambda I\xi\Theta^{\mathrm{T}}\Xi & -2\xi\lambda\Theta^{\mathrm{T}}\Theta + I & & \\
0 & 0 & \lambda I & -\delta^2 I & \\
\Psi^{\mathrm{T}}P & 0 & -\xi\lambda\Psi^{\mathrm{T}}\Theta & 0 & -\delta^2 I
\end{bmatrix}
$$

When $\Omega < 0$, it implies:

$$
\dot{V}(t) + \varepsilon^{\mathrm{T}}(t)\varepsilon(t) - \delta^2\dot{d}^{\mathrm{T}}(t)\dot{d}(t) < 0 \tag{22}
$$

i.e.:

$$
\dot{V}(t) < \delta^2\dot{d}^{\mathrm{T}}(t)\dot{d}(t) - \varepsilon^{\mathrm{T}}(t)\varepsilon(t) \tag{23}
$$

Integrating both sides of this inequality gives:

$$
\int_0^\infty \dot{V}(\tau)\mathrm{d}\tau < \int_0^\infty \delta^2\dot{d}^{\mathrm{T}}(\tau)\dot{d}(\tau)\mathrm{d}\tau - \int_0^\infty \varepsilon^{\mathrm{T}}(\tau)\varepsilon(\tau)\mathrm{d}\tau \tag{24}
$$

or:

$$
V(\infty) - V(0) < \delta^2\|d(t)\|_2^2 - \|\varepsilon(t)\|_2^2 \tag{25}
$$

Under zero initial conditions, it can be obtained that:

$$
V(\infty) < \delta^2\|d(t)\|_2^2 - \|\varepsilon(t)\|_2^2 \tag{26}
$$

This implies:

$$
\|\varepsilon(t)\|_2^2 < \delta^2\|d(t)\|_2^2 \tag{27}
$$

Thus, the analysis of the intermediate observer is completed.

To clarify the observer design procedure, the above work is summarized as follows:

(1) Select fixed values for $\lambda > 0, \delta > 0$ and $\rho > 0$. All other quantities can be taken directly from the model. Substituting these into the LMI and solving $\Omega < 0$ for a feasible solution with MATLAB's LMI Toolbox function feasp yields P and W; the observer gain matrix L is then obtained via $L = P^{-1}W$. Plugging the resulting parameters into observer (15) completes the design.

(2) If $\lambda > 0$ is not pre-specified, its optimal value can also be found by solving the LMI with the *mincx* solver.

Remark 4. The intermediate observer eliminates the dependence on the observer-matching condition and only requires that lumped disturbances (model errors, noise, ageing effects) are bounded. This assumption holds true for all lithium-ion batteries, so it will not fail due to differences in chemical systems, ensuring robust operation even on batteries with distinctly different electrochemical characteristics.

4. Experimental Verification

To verify the effectiveness of the proposed combined intermediate observer and H_∞ method for lithium battery state estimation, an experimental platform was built using a Neware CT4991-60V-30A battery tester. This device can collect battery voltage and current signals in real-time and transmit them to a host computer via a CAN bus. The experiment used Samsung SDI's INR18650-29E lithium-ion battery, with a nominal voltage of 3.65 V and a nominal capacity of 2.85 Ah. The experimental environment was controlled by a Jianheng BT-B1 battery environmental performance test chamber, maintaining the lithium battery under test at a constant temperature of 25°C±1°C. Experiments were conducted under both non-interference and interference conditions, with data processed on the MATLAB/Simulink platform. For the experimental system in this study, γ was estimated to be 0.05, which is consistent with the tuning value in the LMI gain design and smaller than the theoretical upper limit of 0.08, verifying the effectiveness of the bound estimation. The advantages of the proposed method were shown through SoC estimation results and estimation error comparison curves. Figs. 2 and 3 show the input current and terminal voltage under the considered conditions.

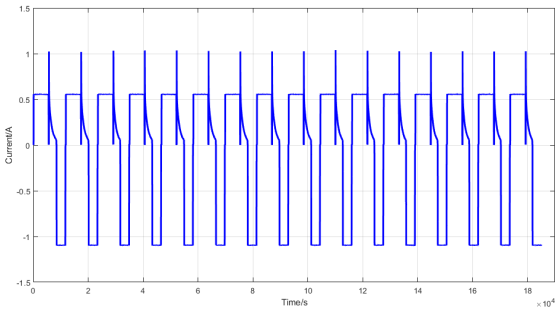

Figure 2. Input Current.

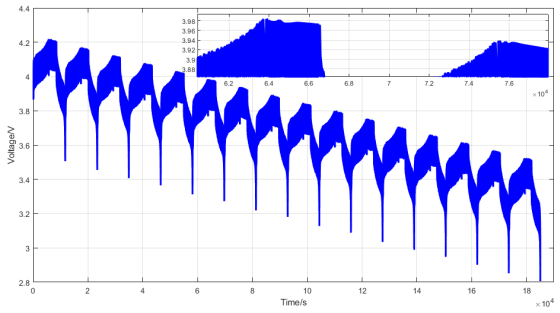

Figure 3. Battery Terminal Voltage.

4.1 Experimental Results without Disturbance

Under disturbance-free experimental conditions, the proposed joint intermediate observer with H_∞ approach (hereinafter referred to as the proposed method) is compared with the traditional H_∞ method. Figs. 4 and 5 show that both methods can satisfactorily estimate the battery SoC, yet they differ markedly in detail. In terms of accuracy, the SoC estimate produced by the proposed method tracks the true value more closely, especially during rapid SoC changes. For example, at the onset of discharge and near the fully-charged state, the estimation error of the proposed method is significantly smaller than that of the H_∞ method. Specifically, the maximum estimation error of the proposed method is 0.015, whereas that of the H_∞ method is 0.032, representing an error reduction of approximately 53 %. Regarding stability, the error curve in Fig. 4 reveals that the proposed method exhibits smaller fluctuations and a smoother profile, indicating superior stability and robustness under disturbance-free conditions. By contrast, the H_∞ method's error curve shows pronounced spikes at certain instants, particularly when the SoC changes rapidly—likely because the H_∞ method is more sensitive to model errors and noise. During long-duration experiments, the estimation error of the proposed method remains consistently low, whereas the error of the H_∞ method gradually increases over time. This demonstrates that the proposed method possesses better long-term stability and can effectively prevent error accumulation.

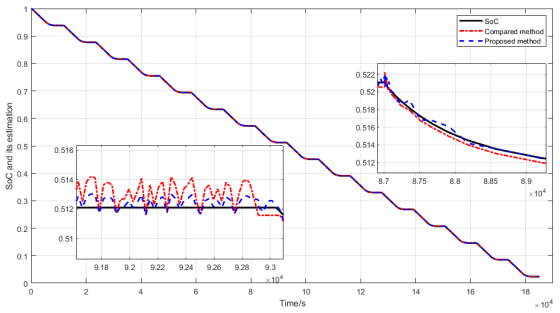

Figure 4. Estimation Results of SoC without Disturbances.

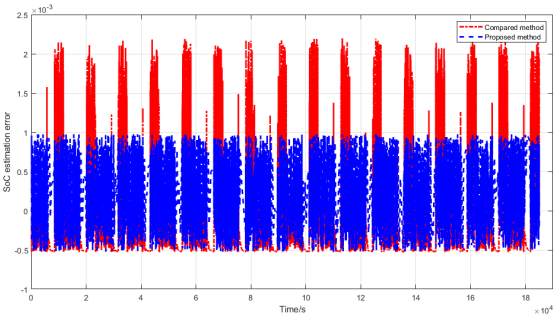

Figure 5. Estimation Error without Disturbances.

4.2 Experimental Results with Disturbance

Under experimental conditions with external disturbances, a 0.1 A peak noise signal is injected into the input current

Table 1
Method Comparison

Operating Condition	Proposed Method	EKF	Conventional H_∞
Maximum SoC Error without Disturbance	1.5 %	2.3 %	3.2 %
Maximum SoC Error with 0.1 A Noise	2.8 %	4.1 %	5.6 %
Average Computational Time per Step	8.2 μs	11.5 μs	9.8 μs

to emulate the sensor noise encountered in practical applications. Figs. 6 and 7 reveal that although both methods are affected, the proposed method retains clear advantages. With respect to disturbance rejection, the proposed method keeps the SoC estimation error low even in the presence of disturbances, registering a maximum error of 0.028, whereas the H_∞ method reaches 0.056. This demonstrates that the proposed method suppresses disturbances more effectively and reduces their impact on the estimate. The error curves in Fig. 6 show that the proposed method exhibits smaller fluctuations and a smoother profile, while the H_∞ method displays pronounced oscillations whenever the disturbance is active; the larger the disturbance, the more volatile the error becomes. Thus, the proposed method maintains superior accuracy and stability under noisy conditions. Furthermore, the proposed method responds more rapidly to rapid SoC changes under disturbances. For instance, at the onset of discharge and near the fully charged state, its estimate tracks the true value almost immediately, whereas the H_∞ method reacts more sluggishly and consequently incurs larger errors.

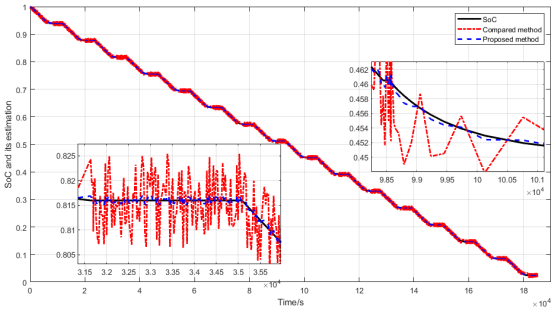

Figure 6. Estimation Results of SoC with Disturbances.

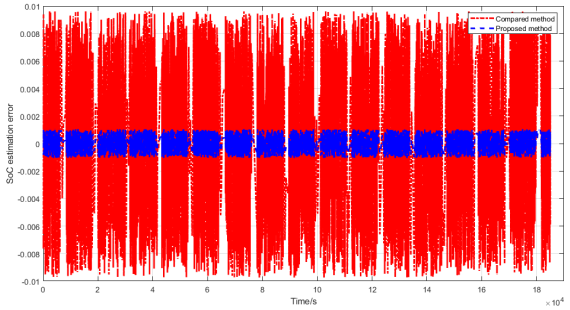

Figure 7. Estimation Error with Disturbances.

4.3 Performance Comparison with Existing Methods

The configuration follows [29]: process-noise covariance $Q = \mathrm{diag}\begin{bmatrix} 10^{-6} & 10^{-6} & 10^{-6} \end{bmatrix}$; measurement-noise covariance $d_2(t) = 10^{-4}$; initial estimation-error covariance $P_0 = \mathrm{diag}\begin{bmatrix} 0.01 & 0.001 & 0.001 \end{bmatrix}$. The comparison results are summarized in Table 1.

In the noise-free case, the proposed method reduces the maximum error by 34.8 % versus EKF and 53.1 % versus H_∞. Under 0.1 A current noise, the proposed method's maximum error is 2.8 %, which is 31.7 % lower than EKF and 50 % lower than H_∞. Computationally, the proposed algorithm requires 8.2 μs per step, outperforming both EKF (11.5 μs) and conventional H_∞ (9.8 μs), making it better suited for embedded BMS implementation.

5. Conclusion

This paper presents an intermediate-observer-based method for SoC estimation of lithium-ion batteries, aimed at enhancing both accuracy and robustness. By integrating a dual-polarization RC equivalentcircuit model with H_∞ techniques, the designed intermediate observer delivers high precision and stability under disturbance-free conditions and exhibits strong disturbance-rejection capability when external noise is present. Experimental results show that the proposed method achieves a maximum estimation error of only 0.015 under no interference, a 53% reduction compared with the conventional H_∞ approach. When disturbances are introduced, the maximum error rises to 0.028 , still significantly outperforming the 0.056 observed with the H_∞ method. Because the proposed scheme does not require the observer-matching condition, it enjoys wider applicability and offers an effective solution for lithium-ion battery SoC estimation. Future work will focus on extending it to extreme temperatures ($-20°\mathrm{C} - 60°\mathrm{C}$) and high-rate (2C−5C) scenarios, and integrating cell inconsistency compensation for battery packs to enhance practicality.

References

[1] M. Yin, "Research on rul of li-ion battery based on improved arpf model," *International Journal of Power and Energy Systems*, vol. 41, no. 1, pp. 58–64, 2021.

[2] H. Obeid, R. Petrone, H. Chaoui, and H. Gualous, "Higher order sliding-mode observers for state-of-charge and state-of-health estimation of lithium-ion batteries," *IEEE Transactions on Vehicular Technology*, vol. 72, no. 4, pp. 4482–4492, 2023.

[3] A. Nath, R. Gupta, R. Mehta, and S. S. Bahga, "Attractive ellipsoid sliding-mode observer design for state of charge esti-

mation of lithium-ion cells," *IEEE Transactions on Vehicular Technology*, vol. 69, no. 12, pp. 14701–14712, 2020.

[4] C. H. Hyun and S. M. Baek, "Hybrid-type intelligent state of charge observer of li-ion batteries," *Journal of Electrical Engineering & Technology*, vol. 16, no. 6, pp. 3017–3024, 2021.

[5] S. Rout and S. Das, "Online state-of-charge estimation of lithium-ion battery using a fault-tolerant and noise-immune threefold modified adaptive extended kalman filter," *IEEE Transactions on Transportation Electrification*, vol. 10, no. 4, pp. 9366–9380, 2024.

[6] C. Y. Pan, Z. X. Peng, and S. C. Yang, "Battery state of charge estimation with event-triggered parameter identification," *IEEE Transactions on Transportation Electrification*, vol. 10, no. 4, pp. 10401–10409, 2024.

[7] N. Li, F. Hu, and W. Ma, "Application of multi-energy composite energy storage system technology in electric vehicles," *International Journal of Power and Energy Systems*, vol. 44, no. 10, pp. 1–10, 2024.

[8] H. D. Xi, X. J. Lin, S. Zhang, and X. Luo, "A lumped disturbance compensation scheme for unbiased state-of-charge estimation of lithium-ion batteries," *IEEE Transactions on Power Electronics*, vol. 40, no. 3, pp. 4569–4580, 2025.

[9] I. M. Monirul, L. Qiu, and R. Ruby, "Accurate state of charge estimation for uav-centric lithium-ion batteries using customized unscented kalman filter," *Journal of Energy Storage*, vol. 107, p. 114955, 2025.

[10] R. Xiong, Q. Yu, W. Shen, and C. Lin, "A sensor fault diagnosis method for a lithium-ion battery pack in electric vehicles," *IEEE Transactions on Power Electronics*, vol. 34, no. 10, pp. 9709–9718, 2019.

[11] L. Yang, T. Liu, Z. Li, and W. Zhou, "State estimation and energy management of microgrid energy storage system using particle filter and markov chain monte carlo," *International Journal of Power and Energy Systems*, vol. 44, no. 10, 2024.

[12] Q. Ouyang, J. Chen, J. Zheng, and Y. Hong, "Soc estimation-based quasi-sliding mode control for cell balancing in lithium-ion battery packs," *IEEE Transactions on Industrial Electronics*, vol. 65, no. 4, pp. 3427–3436, 2018.

[13] M. Naguib, P. Kollmeyer, and A. Emadi, "Lithium-ion battery pack robust state of charge estimation, cell inconsistency, and balancing: Review," *IEEE Access*, vol. 9, pp. 50570–50582, 2021.

[14] Z. Xi, M. Dahmardeh, B. Xia, and Y. Fu, "Learning of battery model bias for effective state of charge estimation of lithium-ion batteries," *IEEE Transactions on Vehicular Technology*, vol. 68, no. 9, pp. 8613–8628, 2019.

[15] Y. Dai, Q. Peng, T. Liu, and J. Meng, "Negative resistor-based equivalent circuit model of lithium-ion battery energy storage system for grid inertia support," *IEEE Transactions on Power Electronics*, vol. 39, no. 11, pp. 15217–15230, 2024.

[16] W. Zhang, L. Wang, L. Wang, and C. Liao, "Joint state-of-charge and state-of-available-power estimation based on the online parameter identification of lithium-ion battery model," *IEEE Transactions on Industrial Electronics*, vol. 69, no. 4, pp. 3677–3688, 2022.

[17] W. Song, R. Liu, X. Jin, and W. Guo, "Soc estimation for lithium-ion batteries based on weighted multi-innovation sage-husa adaptive ekf," *Energies*, vol. 18, no. 16, p. 4364, 2025.

[18] J. Xu, C. C. Mi, B. Cao, and J. Deng, "The state of charge estimation of lithium-ion batteries based on a proportional-integral observer," *IEEE Transactions on Vehicular Technology*, vol. 63, no. 4, pp. 1614–1621, 2014.

[19] M. Y. Zhang and X. B. Fan, "Design of battery management system based on improved ampere-hour integration method," *International Journal of Electric and Hybrid Vehicles*, vol. 14, no. 1-2, pp. 1–29, 2022.

[20] Z. L. Chen, W. J. Liao, and P. F. Li, "Lithium-ion battery state of charge estimation strategy for industrial applications," *Proceedings of the Institution of Civil Engineers - Energy*, vol. 177, no. 1, pp. 14–21, 2023.

[21] G. Z. Dong, G. X. Gao, Y. J. Lou, and J. C. Yu, "Hybrid physics and data-driven electrochemical states estimation for lithium-ion batteries," *IEEE Transactions on Energy Conversion*, vol. 39, no. 4, pp. 2689–2700, 2024.

[22] M. Savargaonkar, I. Oyewole, A. Chehade, and A. A. Hussein, "Uncorrelated sparse autoencoder with long short-term memory for state-of-charge estimations in lithium-ion battery cells," *IEEE Transactions on Automation Science and Engineering*, vol. 21, no. 1, pp. 15–26, 2024.

[23] D. D. Ge, G. Y. Jin, J. Q. Wang, and Z. D. Zhang, "A novel ba-abc-elm model for estimating state of health of lithium-ion batteries," *Energy Reports*, vol. 13, pp. 465–476, 2025.

[24] A. Elachhab, E. Laadissi, A. Tabine, and A. Hajjaji, "Deep learning and data augmentation for robust battery state of charge estimation in electric vehicles," *Electrical Engineering*, vol. 107, pp. 7313–7327, 2025.

[25] Z. D. Lu, H. M. Chen, and F. X. Xu, "State of charge estimation of lithium-ion battery based on tscso-gru-attention," *International Journal of Green Energy*, vol. 22, no. 8, pp. 1628–1638, 2024.

[26] A. V. Vykhodtsev, D. Jang, Q. Wang, W. Rosehart, and H. Zareipour, "Physics-aware degradation model of lithium-ion battery energy storage for techno-economic studies in power systems," *IEEE Transactions on Sustainable Energy*, vol. 15, no. 1, pp. 316–327, 2024.

[27] C. S. Huang and M. Y. Chow, "Robust state-of-charge estimation for lithium-ion batteries over full soc range," *IEEE Journal of Emerging and Selected Topics in Industrial Electronics*, vol. 2, no. 3, pp. 305–313, 2021.

[28] T. Y. Meng, Z. L. Lin, Y. Wan, and Y. A. Shamash, "Nonlinear observer-based state-of-charge balancing of networked battery energy storage systems," *Journal of Control and Decision*, vol. 12, no. 1, pp. 49–64, 2025.

[29] F. Yang, Q. Mao, J. M. Zhang, and S. L. Hou, "Real-time state-of-charge estimation for rechargeable batteries based on in-situ ultrasound-based battery health monitoring and extended kalman filtering model," *Applied Energy*, vol. 381, p. 125161, 2025.

[30] Y. Feng, C. Xue, Q. L. Han, and F. L. Han, "Robust estimation for state-of-charge and state-of-health of lithium-ion batteries using integral-type terminal sliding-mode observers," *IEEE Transactions on Industrial Electronics*, vol. 67, no. 5, pp. 4013–4023, 2020.

[31] A. Clemente, A. Cecilia, and R. Costa-Castelló, "Online state of charge estimation for a vanadium redox flow battery with unequal flow rates," *Journal of Energy Storage*, vol. 60, p. 106503, 2023.

Biographies

Dan Wang received her Bachelor's degree in Computer Science and Technology from Northeast Electric Power University (NEPU). She is currently affiliated with State Grid Liaoning Electric Power Co. Ltd., Shenyang, Liaoning, China. Her research interests include the application of artificial intelligence in the field of measurement.

Sicheng Zhou received his B.E. degree in Electrical Engineering and Automation from Dalian Jiaotong University in 2010. He is currently affiliated with State Grid Liaoning Electric Power Co. Ltd., Shenyang, Liaoning, China. His research interests include electrical energy metering and instrument detection.

Zhibo Feng received his Master's degree from Northeast Electric Power University, China. He is currently affiliated with State Grid Liaoning Electric Power Co. Ltd., Shenyang, Liaoning, China. His research interests include the application of artificial intelligence in the field of measurement.

Jun Wu received her Master of Engineering degree in Measurement and Testing Technology and Instruments from Shenyang University of Technology in 2012. She is currently affiliated with State Grid Liaoning Electric Power Co. Ltd., Shenyang, Liaoning, China. Her research interests include electrical energy metering, measurement and detection technology, and related applications.

Guanjie Wang graduated in Environmental Engineering from Zhejiang University of Technology. He is currently a postdoctoral fellow at the Taizhou Institute of Zhejiang University, Taizhou, Zhejiang, China. His research interests include incineration flue gas pollution control, resource utilization of waste incineration fly ash, and the development of environmental functional materials.